MODELING OF CROSS-REGULATION IN MULTIPLE-OUTPUT FLYBACK CONVERTERS

Dragan Maksimović and Robert Erickson
Colorado Power Electronics Center
Department of Electrical and Computer Engineering
University of Colorado, Boulder, CO 80309-0425
http://ece-www.colorado.edu/~pwrelect
Phone: (303)492-4863, Fax: (303)492-2758, maksimov@colorado.edu, rwe@schof.colorado.edu

Abstract – **In this paper, complex operation of multiple-output flyback converters is explained in terms of the extended cantilever magnetics model. Analytical results are derived that can accurately predict steady-state cross-regulation properties of a converter with any number of outputs and with arbitrarily complex magnetics configuration. Two snubber configurations are considered: a passive voltage-clamp snubber and an active-clamp snubber. Predictions of the model are verified by experiments. The analytical models are the basis for a discussion of magnetics design guidelines that can result in improved cross-regulation in multiple-output flyback converters.**

1 Introduction

The multiple-output flyback converter such as the example shown in Fig. 1 is one of the most frequently used configurations in low-cost, relatively low power applications. If all windings are perfectly coupled, and if conduction losses are small, the output voltages in continuous conduction mode are simply proportional to the respective turns ratios and closed-loop regulation of one output results in perfect regulation of all outputs. In practice, however, perfect coupling is impossible to achieve, the observed operation is much more complex, and poor cross-regulation results are often obtained.

Poor cross-regulation can only in part be attributed to conduction losses. If an output is heavily loaded, its output drops due to increased voltage drops across conducting devices and winding resistances. If this output is closed-loop regulated, the duty ratio increases to compensate for the load-induced voltage drop, and all other unregulated output voltages increase accordingly. Conduction losses and their effects on cross-regulation in a multiple-output converter can be modeled using standard averaging techniques.

It has been recognized that transformer leakage inductances play the key role in operation of a multiple-output flyback converter [1, 2, 3]. Previous analyses were limited to a two-output case, or were based on simplifying assumptions about the transformer model. Transformer leakage inductances are usually considered second-order effects, and any analysis that would attempt to take their effects into account would yield intractable results, especially if the transformer had more than two secondary windings. However, secondary current waveforms and the steady-state solution in the converter are in fact very strongly dependent on the transformer leakages. Because of the complex converter operation, and lack of general and complete magnetics model suitable for cross-regulation analysis, very few results are now available to aid the designer.

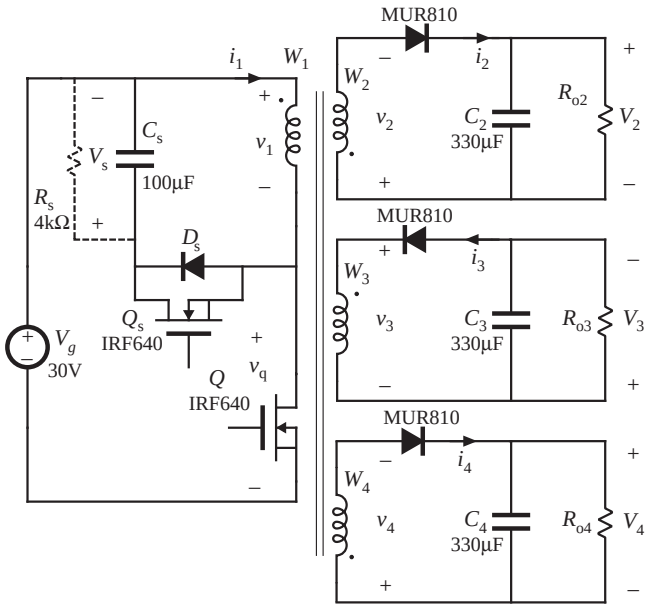

Figure 1: Experimental 3-output flyback converter with passive or active-clamp snubber.

The purpose of this paper is to give complete qualitative and quantitative explanation of the multiple-output flyback converter operation, and to derive steady-state cross-regulation models valid for any number of outputs and arbitrarily complex magnetics. Our analysis is based on the extended cantilever magnetics model [4], which has earlier been applied to modeling cross-regulation in forward-type converters with coupled inductors [5].

In Section 2, the extended cantilever model is briefly described using a flyback transformer example for the experimental converter in Fig. 1. General analytical results that give predictions of steady-state output voltage variations as functions of load currents in a converter with arbitrary number of outputs are derived in Section 3. The results are obtained for a converter with a passive voltage-clamp snubber, and for a converter with an active-clamp snubber. Experimental ver-

ification of the cross-regulation models is presented in Section 4. In Section 5 we discuss model implications and design guidelines.

2 Extended cantilever magnetics model: experimental example

The extended cantilever model is a general circuit model for multiple-winding magnetics [4]. Fig. 2 shows the winding geometry and the corresponding extended cantilever model for the transformer used in the experimental 3-output, 100kHz flyback converter of Fig. 1. The model parameters are a magnetizing inductance L_{11}, effective leakage inductances l_{ij} between the windings, and effective turns ratios n_j. The model can be used for arbitrarily complex magnetics with any number of windings. Most importantly, the leakage inductances that are essential for analyses and design of multiple-output converters are directly exposed in the model, and all model parameters can be directly measured, as described in [4].

Leakage inductance values in the model can be related to the winding geometry. Winding W_4 occupies a small portion of the bobbin, and is farthest away from the primary winding W_1. As a result, the effective leakage inductance l_{14} is relatively large. Winding W_2 is closest to the primary and the effective leakage inductance l_{12} is the smallest of the three primary-to-secondary leakage inductances. Notice that a leakage inductance in the model can have a negative value. In Fig. 2, l_{34} is negative. This can be related to the winding arrangement where the W_4 current and the current induced in the W_2 winding result in the opposite polarity of the induced W_3 current [4].

In the experimental converter, the input is $V_g = 30$V, and the nominal outputs are: $V_2 = V_3 = +12$V, $V_4 = 3.3$V. The 3.3V (winding W_4) output is taken to be the main output that would be regulated by a feedback loop, while V_2 (winding W_2) and V_3 (winding (W_3) are auxiliary outputs.

3 Modeling of cross-regulation in multiple-output flyback converters

Multiple-output flyback converters have complex operation and characteristics that strongly dependent on the transformer leakage inductances. Secondary currents can have positive or negative slopes, and multiple discontinuous conduction modes may occur depending on operating conditions and relative values of leakage inductances. Changes in the load current at one of the outputs strongly affect all output voltages.

This section has two main objectives: (1) to qualitatively explain complex operation of a multiple-output flyback converter using equivalent circuit models based on the extended cantilever magnetics model; (2) to derive analytical results that can be used to predict how load variations at one output affect voltage variations at any other output.

To derive general results valid for any number of outputs, it is convenient to use matrix/vector notation. For a three-output example,

$$\mathbf{V}=\begin{bmatrix} V_2 \\ V_3 \\ V_4 \end{bmatrix}, \mathbf{V}'=\begin{bmatrix} V_2/n_2 \\ V_3/n_3 \\ V_4/n_4 \end{bmatrix}, \mathbf{I}=\begin{bmatrix} I_2 \\ I_3 \\ I_4 \end{bmatrix}, \mathbf{I}'=\begin{bmatrix} n_2 I_2 \\ n_3 I_3 \\ n_4 I_4 \end{bmatrix}, \quad (1)$$

are the vectors of output voltages and currents, referred to the secondary or the primary side, respectively. The reference polarities for the currents and voltages are as shown in Figs. 1 and 2.

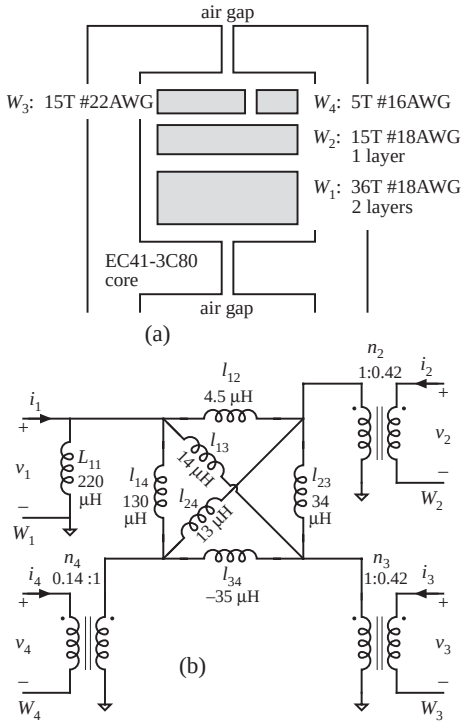

Figure 2: Winding geometry (a) and the extended cantilever model (b) of the transformer used in the flyback converter of Fig. 1.

The steady-state cross-regulation models we derive in this section will show how changes in the DC load currents $\Delta\mathbf{I}$ produce variations in the DC output voltages $\Delta\mathbf{V}$:

$$\Delta\mathbf{V} = -\mathbf{R}\Delta\mathbf{I}\,, \quad (2)$$

where $\mathbf{R}$ is a matrix of Thevenin equivalent output resistances for a given DC operating point. In the analysis and discussion of cross-regulation properties, it is often useful to express the model (2) in terms of the voltages and currents referred to the primary side:

$$\Delta\mathbf{V}' = -(\mathbf{N}^{-1}\mathbf{R}\mathbf{N}^{-1})\Delta\mathbf{I}' = -\mathbf{R}'\Delta\mathbf{I}' \quad (3)$$

where $\mathbf{N}$ is a diagonal matrix with the effective turns ratios n_2, n_3, etc., on the main diagonal. In general, it is clear that smaller entries in $\mathbf{R}'$ result in better cross-regulation. Because of the leakage inductances, however, the output resistances are nonzero even if all conduction losses are neglected. One should also note that perfect closed-loop cross-regulation can be achieved even with non-zero output resistances. For example, suppose that two rows of $\mathbf{R}'$ have equal terms, so that arbitrary load variations result in the same voltage variations (referred to the primary) on both outputs corresponding to these rows. Then, if one of the two outputs is closed-loop regulated, the other output will be tightly regulated as well.

The models derived in this section will show how $\mathbf{R}'$ and $\mathbf{R}$ can be found in general, in terms of the transformer extended cantilever model.

Referring to Fig. 1, we consider multiple-output flyback converters with two commonly used snubber configurations: (1) a passive voltage-clamp snubber where a resistor R_s loads the snubber capacitor C_s, and the auxiliary device Q_s is removed, and (2) an active-clamp

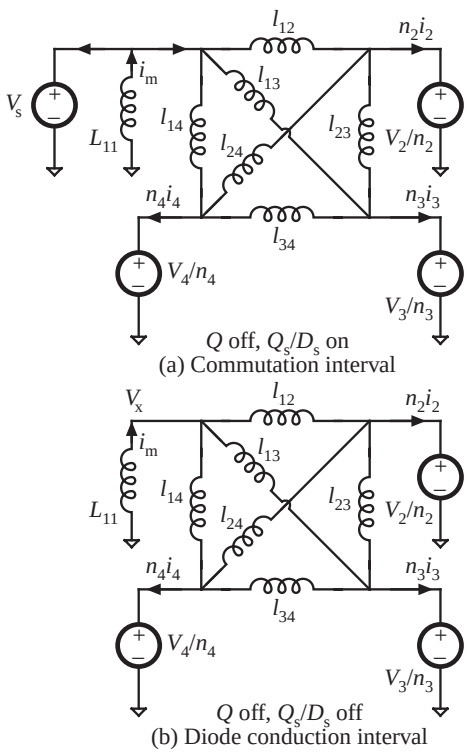

Figure 3: Circuit model during parts of the switching cycle when the main switch Q is off: (a) the commutation interval and (b) the diode conduction interval.

snubber where the snubber resistor R_s is removed and the auxiliary device Q_s is used to enable bidirectional current flow to and from the snubber capacitor C_s. Steady-state solution and cross-regulation model parameters in these two cases can be significantly different.

3.1 Multiple-output flyback converter with passive voltage-clamp snubber

The converter operation is explained with reference to the circuit models shown in Fig. 3 and the idealized waveforms shown in Fig. 4. A set of experimental waveforms observed with the passive voltage-clamp snubber in the experimental converter of Fig. 1 is shown in Fig. 5.

When the transistor Q turns off, a commutation interval starts when the snubber diode D_s turns on, conducting the magnetizing current i_m and clamping the primary voltage to $v_1 = -V_s$. The secondary-side diodes also begin conducting. The circuit model during the commutation interval is shown in Fig. 3(a). A secondary current increases at the rate determined by the snubber voltage V_s, the output voltages, and the effective leakage inductances. For example, for the winding W_2 current, we have:

$$n_2 \frac{di_2}{dt} = \frac{V_s - V_2/n_2}{l_{12}} + \frac{V_3/n_3 - V_2/n_2}{l_{23}} + \frac{V_4/n_4 - V_2/n_2}{l_{24}}, \quad (4)$$

and similar expressions can be written for the other winding currents. Given that the reflected output voltages are nearly equal, $V_2/n_2 \approx V_3/n_3 \approx V_4/n_4$, the rate of change is dominated by the first term,

$$n_2 \frac{di_2}{dt} \approx \frac{V_s - V_2/n_2}{l_{12}}. \quad (5)$$

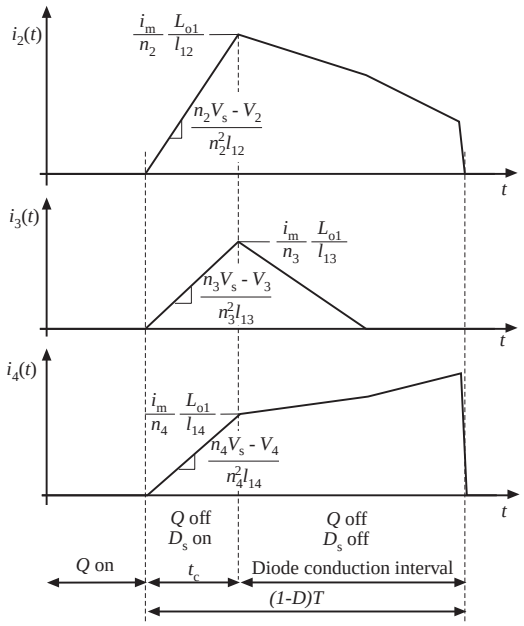

Figure 4: Idealized secondary current waveforms in the converter with a passive voltage-clamp snubber.

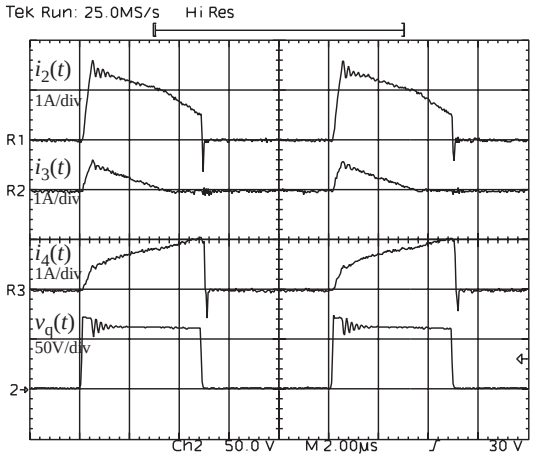

Figure 5: Experimental waveforms in the flyback converter with the passive voltage-clamp snubber at the operating point: $D = 0.52$, $V_2 = 13.5$V, $V_3 = 14.2$V, $V_4 = 3.4$V, $R_{o2} = 25\Omega$, $R_{o3} = 150\Omega$, $R_{o4} = 11\Omega$.

Therefore, during the commutation interval t_c, the secondary currents increase at the rates determined by the effective leakage inductances l_{12}, l_{13}, and l_{14}, as shown in Fig. 4. These rates are not directly related to the individual load currents. At the end of the commutation interval t_c, the sum of the reflected secondary currents becomes equal to the magnetizing current i_m,

$$n_2 i_2 + n_3 i_3 + n_4 i_4 = i_m, \quad (6)$$

and the snubber diode D_s turns off. The values of the individual secondary winding currents at this time are determined by the relative values of l_{12}, l_{13}, and l_{14}, and again are not directly related to the

individual load currents,

$$n_k i_k = \frac{L_{o1}}{l_{1k}} i_m, \tag{7}$$

where

$$L_{o1} = l_{12} || l_{13} || l_{14}, \tag{8}$$

and $k = 1, 2, 3$. In the magnetics example of Fig. 2, winding W4 is poorly coupled to the primary and l_{14} is relatively large. As a result, the current i_4 at the end of the commutation is relatively small. Since winding W_2 and W_3 are better coupled to the primary, the currents i_2, i_3 at the end of the commutation interval are relatively large, as illustrated by the experimental waveforms in Fig. 5.

During the remainder of the switching period, which is called here the diode conduction interval, the secondary currents increase or decrease at the rates that depend on the differences between the reflected output voltages, and the voltage V_x across the magnetizing inductance. The circuit model during the diode conduction interval is shown in Fig. 3(b). If an output is heavily loaded and the current at the end of the commutation interval is relatively small, the slope of the corresponding winding current will be positive, which means that the corresponding output voltage is reduced. In Fig. 5, this can be observed in the i_4 current of the V_4 output. Since the currents i_2, i_3 at the end of the commutation interval are relatively large and since these outputs are not heavily loaded, the corresponding winding currents *decrease* during the diode-conduction interval, which indicates that the reflected output voltages V_2/n_2, V_3/n_3 must be greater than V_x. From this qualitative discussion, it follows immediately that because of the transformer leakage inductances, each output exhibits a nonzero output resistance, even in continuous conduction mode, and even if all losses are neglected.

During the diode conduction interval, the rates of change of the reflected secondary currents are

$$\frac{d\mathbf{i}'}{dt} = \mathbf{B}_1(\mathbf{V}' - \mathbf{u}V_x), \tag{9}$$

where

$$\mathbf{B}_1 = \begin{bmatrix} -\frac{1}{L_{o2}} & \frac{1}{l_{23}} & \frac{1}{l_{24}} \\ \frac{1}{l_{23}} & -\frac{1}{L_{o3}} & \frac{1}{l_{34}} \\ \frac{1}{l_{24}} & \frac{1}{l_{34}} & -\frac{1}{L_{o4}} \end{bmatrix}, \tag{10}$$

$\mathbf{u}^T = \begin{bmatrix} 1 & 1 & 1 \end{bmatrix}$, and

$$L_{o2} = l_{12} || l_{23} || l_{24}, \tag{11}$$

$$L_{o3} = l_{13} || l_{23} || l_{34}, \tag{12}$$

$$L_{o4} = l_{14} || l_{24} || l_{34}, \tag{13}$$

are the Thevenin equivalent output inductances of the secondary windings, referred to the primary side.

The secondary winding currents may have positive or negative slopes. A winding current with negative slope may drop to zero before the end of the diode conduction interval (for example, see current i_3 in Fig. 5), which results in a discontinuous conduction mode and even larger variations in the output voltages. In general, depending on the load conditions and values of the magnetics model parameters, an output may operate in continuous or discontinuous mode, which adds to the complexity of the converter operation. We first derive a steady-state cross-regulation model assuming that all outputs operate in the continuous conduction mode.

Assuming that the commutation interval t_c is a small fraction of the switching period, averaging of a secondary winding current over a switching period gives a relation that includes the initial value of the current i_k at the start of the diode conduction interval, which is given by (7), the rate of change of the current, which is given by (9), and the average output current I_k,

$$I_k \approx (1-D) i_k + (1-D)^2 \frac{1}{2 f_s} \frac{di_k}{dt}. \tag{14}$$

The magnetizing current i_m at the end of the commutation interval is related to the load currents:

$$\begin{aligned} i_m &\approx I_m + \frac{V_x(1-D)}{2 L_{11} f_s} \\ &\approx \frac{1}{1-D}\left(n_2 I_2 + n_3 I_3 + n_4 I_4\right) + \frac{V_x(1-D)}{2 L_{11} f_s} \\ &= \frac{1}{1-D}(\mathbf{u}^T \mathbf{I}') + \frac{V_x(1-D)}{2 L_{11} f_s}. \end{aligned} \tag{15}$$

Combining (7), (9), (14), and (15) yields the steady-state solution for the reflected DC output voltages $\mathbf{V}'$ in terms of the reflected load currents $\mathbf{I}'$ and the duty ratio D:

$$\mathbf{B}_1(\mathbf{V}' - \mathbf{u}V_x) = \frac{2 f_s}{(1-D)^2} \mathbf{B}_2 \mathbf{I}' - \mathbf{b}_2 \frac{L_{o1}}{L_{11}} V_x, \tag{16}$$

where $\mathbf{B}_1$ is given by (10),

$$\mathbf{B}_2 = \begin{bmatrix} 1 - \frac{L_{o1}}{l_{12}} & -\frac{L_{o1}}{l_{12}} & -\frac{L_{o1}}{l_{12}} \\ -\frac{L_{o1}}{l_{13}} & 1 - \frac{L_{o1}}{l_{13}} & -\frac{L_{o1}}{l_{13}} \\ -\frac{L_{o1}}{l_{14}} & -\frac{L_{o1}}{l_{14}} & 1 - \frac{L_{o1}}{l_{14}} \end{bmatrix}, \tag{17}$$

and

$$\mathbf{b}_2 = \begin{bmatrix} \frac{1}{l_{12}} \\ \frac{1}{l_{13}} \\ \frac{1}{l_{14}} \end{bmatrix}. \tag{18}$$

Voltage V_x across the magnetizing inductance L_{11} during the diode conduction interval can be found from the volt-second balance on L_{11},

$$V_x = \frac{D V_g - V_s t_c f_s}{1 - D - t_c f_s} \approx \frac{D V_g - L_{o1} i_m f_s}{1-D}, \tag{19}$$

assuming that the commutation interval t_c is short compared to $(1-D)T$, and that the voltage across the effective primary-to-secondary leakage inductances during the commutation interval is approximately equal to the snubber voltage V_s.

From (15) and (19), and using $L_{o1} << L_{11}$, it follows that

$$V_x \approx V_g \frac{D}{1-D} - \frac{f_s L_{o1}}{(1-D)^2}(\mathbf{u}^T \mathbf{I}') \tag{20}$$

The steady-state solution (16), (20) is a general result that shows how the dc output voltages depend on the dc load currents in a multiple-output flyback converter with any number of outputs and with arbitrarily complex magnetics.

For a given DC operating point, the matrix of Thevenin equivalent output resistances follows from (3), (16) and (20):

$$\mathbf{R}' = -\frac{2 f_s}{(1-D)^2}\left(\mathbf{B}_1^{-1}\mathbf{B}_2 + \frac{L_{o1}}{2}(\mathbf{B}_1^{-1}\mathbf{b}_2 \frac{L_{o1}}{L_{11}} - \mathbf{u})\mathbf{u}^T\right) \tag{21}$$

Assuming that effective leakage inductances are of the same order of magnitude, and that $L_{o1} << L_{11}$, the expression for $\mathbf{R}'$ can be simplified:

$$\mathbf{R}' = -\frac{2f_s}{(1-D)^2}\left(\mathbf{B}_1^{-1}\mathbf{B}_2 - \frac{L_{o1}}{2}\mathbf{u}\mathbf{u}^T\right) \tag{22}$$

Here, $\mathbf{B}_1$ (given by (10)), $\mathbf{B}_2$ (given by (17)), and L_{o1} (given by (8)), all depend only on the extended cantilever magnetics model parameters. The output resistances are directly proportional to the switching frequency f_s, which is not surprising since the output resistances are related to the impedances of the transformer leakage inductances. Also, one may note that the output resistances depend on the steady-state operating point through the duty ratio D. When the converter is operated open loop at constant duty ratio D, the output resistances are constant, and the model predicts that output voltage variations are linear functions of load variations.

In the analysis above, we assumed that all outputs operate in the continuous conduction mode (CCM). It is of interest to find a condition for CCM operation because even larger variations in output voltages can be expected if an output moves from CCM to discontinuous conduction mode (DCM).

For a secondary winding, the condition for operation in CCM is that the peak current ripple is smaller than the average value during the diode conduction interval. In vector form,

$$\frac{\mathbf{I}'}{1-D} + \frac{1-D}{2f_s}\frac{d\mathbf{i}'}{dt} > 0 \tag{23}$$

The relation between the current slopes and the average currents can be deduced from (9) and (16),

$$\frac{d\mathbf{i}'}{dt} = \frac{2f_s}{(1-D)^2}\mathbf{B}_2\mathbf{I}' - \mathbf{b}_2\frac{L_{o1}}{L_{11}}V_x. \tag{24}$$

Eqs. (23) and (24) yield the CCM condition:

$$\begin{bmatrix} 2\frac{l_{12}}{L_{o1}} - 1 & -1 & -1 \\ -1 & 2\frac{l_{13}}{L_{o1}} - 1 & -1 \\ -1 & -1 & 2\frac{l_{14}}{L_{o1}} - 1 \end{bmatrix} \mathbf{I}' > \frac{(1-D)^2 V_x}{2f_s L_{11}}\mathbf{u}. \tag{25}$$

Note that the CCM condition for each output depends not only on the output's load current but also on the load currents at the other outputs. Increasing the load current on one output eventually drives the other outputs into discontinuous conduction mode. This is because increasing the load current on one output increases the magnetizing current (as shown by (15)), which in turn increases the currents at the end of the commutation interval on all outputs (as shown by (7)). For an output with constant load, the larger initial value at the start of the diode conduction interval implies that the final value at the end of the diode conduction interval must decrease. If the winding current drops to zero before the end of the diode conduction interval, this output enters discontinuous conduction mode. The result (25) quantifies this behavior.

3.2 Multiple-output flyback converter with active-clamp snubber

If an active-clamp snubber is used, the voltage v_1 is clamped to V_s during the entire interval when the main transistor Q is off. The commutation interval and the diode conduction interval merge into one interval of length $(1-D)T$, with the equivalent circuit model shown in Fig. 3(a). Idealized secondary current waveforms are shown in Fig. 6. As an example, Fig. 7 shows experimental waveforms for the same operating conditions as in Fig. 5, but with the active-clamp snubber. Note that the secondary current waveshapes are significantly different than in the passive-snubber case.

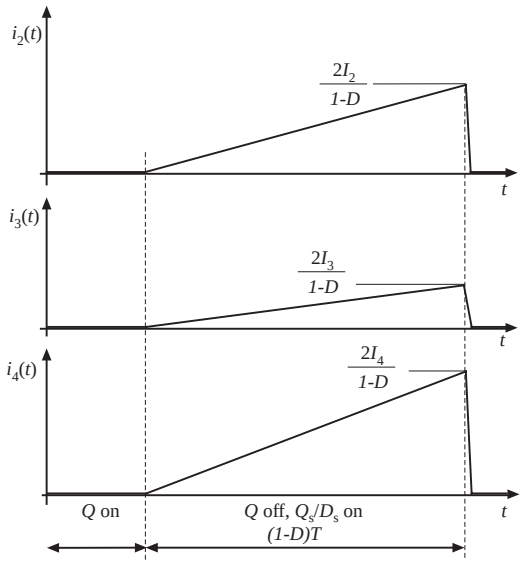

Figure 6: Idealized secondary current waveforms in the converter with an active-clamp snubber.

With the active-clamp snubber, all outputs can operate only in continuous conduction mode, which simplifies the analysis. The secondary currents start from zero and increase at the rates that depend on leakage inductances and differences between reflected output voltages:

$$\frac{d\mathbf{i}'}{dt} = \mathbf{B}_1(\mathbf{V}' - \mathbf{u}V_s). \tag{26}$$

Winding currents at the end of the diode conduction interval can be easily related to the DC load currents, as shown in Fig. 6, and to the current slopes from (26). This gives a general steady-state solution:

$$\mathbf{B}_1(\mathbf{V}' - \mathbf{u}V_s) = \frac{2f_s}{(1-D)^2}\mathbf{I}' \tag{27}$$

where

$$V_s = \frac{D}{1-D}V_g \tag{28}$$

follows immediately from the volt-second balance on L_{11}.

The output resistance matrix $\mathbf{R}'$ is obtained directly from (27):

$$\mathbf{R}' = -\frac{2f_s}{(1-D)^2}\mathbf{B}_1^{-1}. \tag{29}$$

It can be compared to the result (22) obtained for the passive snubber case. Because of the absence of the commutation interval and discontinuous modes, operation and the steady-state model of a multiple output flyback converter with active-clamp snubber are simpler.

4 Experimental verification of the cross-regulation models

In this section, various predictions of the cross-regulation models derived in Section 3 are compared with experimental results obtained

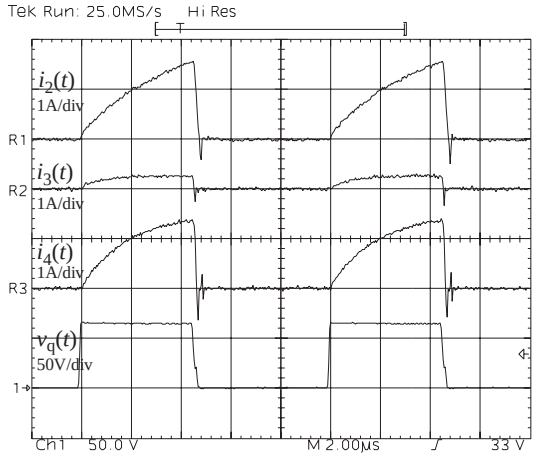

Figure 7: Experimental waveforms in the flyback converter with the active-clamp snubber at the operating point: $D = 0.52$, $V_2 = 13.5$V, $V_3 = 14.2$V, $V_4 = 3.4$V, $R_{o2} = 25\Omega$, $R_{o3} = 150\Omega$, $R_{o4} = 11\Omega$.

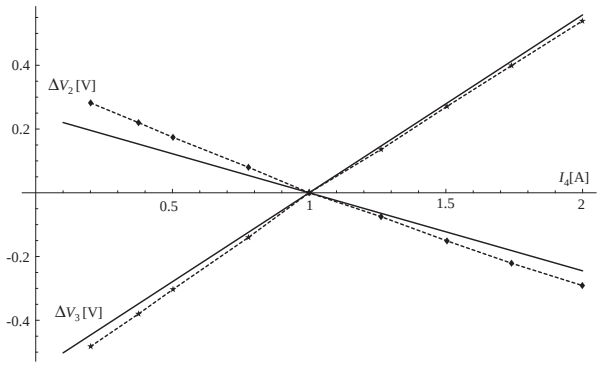

Figure 8: Predicted (solid lines) and experimental (dotted lines) cross-regulation $\Delta V_2(I_4)$ and $\Delta V_3(I_4)$ for the case when the auxiliary outputs operate at $I_2 = I_3 = 0.4$A, and the main output load varies between $I_4 = 0.2$A and $I_4 = 2$A. The converter is operated open-loop at $f_s = 100$kHz, $D = 0.52$.

on the converter in Fig. 1 with the transformer configuration and model shown in Fig. 2.

We first consider the case when the converter is operated with the passive voltage-clamp snubber. Fig. 8 compares the results predicted by the model with experimental results for the case when the auxiliary outputs V_2, V_3 are loaded at $I_2 = I_3 = 0.4$A and the main output load varies between $I_4 = 0.2$A and $I_4 = 2$A. The converter is operated open-loop at constant duty ratio $D = 0.52$. Throughout this load range on the V_4 output, all outputs operate in the continuous conduction mode. One may observe that output voltage variations ΔV_2, ΔV_3 are linear functions of the load I_4, as predicted by the model. The model also correctly predicts that the output V_2 decreases and the output V_3 increases with increasing load on the V_4 output. Although our cross-regulation model included only magnetics parameters while conduction and other losses were neglected, the predicted results correlate very well with the experiments.

At the operating point $D = 0.52$, $I_2 = I_3 = 0.4$A, $I_4 = 1$A, the output resistance matrix (referred to the primary side) is found from (22):

$$\mathbf{R}' = \begin{bmatrix} 2.4 & -1.8 & 4.1 \\ -1.8 & 12.2 & -9.5 \\ 4.1 & -9.5 & 27.4 \end{bmatrix} \Omega \tag{30}$$

and referred to the secondaries,

$$\mathbf{R} = \mathbf{N}\mathbf{R}'\mathbf{N} = \begin{bmatrix} 0.42 & -0.32 & 0.24 \\ -0.32 & 2.15 & -0.56 \\ 0.24 & -0.56 & 0.54 \end{bmatrix} \Omega \tag{31}$$

The measured output resistance matrix is:

$$\mathbf{R}_{\text{experiment}} = \begin{bmatrix} 1.22 & -0.2 & 0.24 \\ -0.35 & 3.2 & -0.52 \\ 0.26 & -0.56 & 0.90 \end{bmatrix} \Omega \tag{32}$$

One can observe very good correlation between predicted and measured off-diagonal terms. This indicates that the coupling terms are indeed determined mainly by the transformer leakage inductances. The diagonal terms, which are the Thevenin equivalent resistances of the individual outputs, are affected by the winding and diode conduction losses, which were not included in the model. Hence, the measured terms on the main diagonal are higher than the values obtained from the model.

In the experimental example, the CCM condition (25) results in:

$$\begin{bmatrix} 0.73 & -0.42 & -0.14 \\ -0.42 & 3.0 & -0.14 \\ -0.42 & -0.42 & 10.9 \end{bmatrix} \begin{bmatrix} I_2 \\ I_3 \\ I_4 \end{bmatrix} > \begin{bmatrix} 0.17\text{A} \\ 0.17\text{A} \\ 0.17\text{A} \end{bmatrix}. \tag{33}$$

The V_2 output has the smallest term (0.73) on the main diagonal, and is most likely to operate in DCM because the winding W_2 is best coupled to the primary, i.e., because the leakage l_{12} in the magnetics model of Fig. 2 is smaller than l_{13} or l_{14}. In general, increasing load on one output while keeping the other two loads constant causes this output to move from DCM to CCM, and the other two outputs to move from CCM to DCM. For example, for $I_2 = 0.6$A, $I_4 = 1$A, and $D = 0.52$, the model prediction is that all outputs operate in CCM for $0.19\text{A} < I_3 < 0.32\text{A}$. In the experimental prototype the V_3 output entered DCM when I_3 dropped below 0.21A, while the V_2 output entered DCM once I_3 exceeded 0.45A.

Next, we consider the experimental converter of Fig. 1 with the active-clamp snubber. At the same operating point as in the passive snubber case, $D = 0.52$, $I_2 = I_3 = 0.4$A, $I_4 = 1$A, the output resistance matrix (referred to the primary side) is found from (29):

$$\mathbf{R}' = \begin{bmatrix} 3.8 & -0.4 & 5.5 \\ -0.4 & 13.6 & -8.1 \\ 5.5 & -8.1 & 28.7 \end{bmatrix} \Omega \tag{34}$$

and referred to the secondaries,

$$\mathbf{R} = \mathbf{N}\mathbf{R}'\mathbf{N} = \begin{bmatrix} 0.67 & -0.07 & 0.33 \\ -0.07 & 2.40 & -0.48 \\ 0.33 & -0.48 & 0.56 \end{bmatrix} \Omega \tag{35}$$

Some of the output resistance values are significantly different compared to the passive-snubber case. This example shows that even

changes in the snubber configuration or snubber parameters can have significant effects on the cross-regulation performance of the flyback converter.

The measured output resistance matrix is:

$$\mathbf{R}_{\text{experiment}} = \begin{bmatrix} 1.5 & -0.3 & 0.25 \\ -0.16 & 3.3 & -0.64 \\ 0.25 & -0.7 & 0.90 \end{bmatrix} \Omega \qquad (36)$$

Conclusions are similar as in the passive snubber case: off-diagonal terms in the model correlate well with the experiments, while the terms on the main diagonal are higher because of the conduction losses which were not included in the model.

5 Design considerations

In Section 3, we have shown that complex behavior of a multiple-output flyback converter can be explained in terms of the extended cantilever magnetics model. The general steady-state solutions (16), (22) and (27), (29) allow one to determine the steady-state cross-regulation performance for any given magnetics design, and a given converter configuration with arbitrary number of outputs. Furthermore, using the derived analytical results, various magnetics design approaches can be evaluated and compared. Several general design guidelines to improve cross-regulation can be deduced:

- Output resistances are directly proportional to leakage inductances (l_{23}, l_{24}, l_{34}) between the secondaries. Therefore, tighter coupling between the secondaries yields improved cross-regulation.
- Minimization of leakage inductances between the secondaries and the primary is not essential for good cross-regulation. In fact, larger l_{12}, l_{13}, l_{14} inductances increase the CCM load ranges, which may improve cross-regulation.
- Relative values of the effective leakage inductances between the primary and the secondaries (l_{12}, l_{13}, l_{14}), are important for good cross-regulation and the best windings arrangement depends on the specified load ranges at the outputs. The winding of the output with the widest load range should have the best coupling to the primary, i.e. it should have the smallest value of the effective leakage inductance.
- Winding arrangements that result in matching rows of the output resistance matrix $\mathbf{R}'$ referred to the primary lead to good closed-loop cross-regulation even if leakage inductances are relatively large. If two outputs have the same terms in the corresponding rows of the $\mathbf{R}'$ matrix, closed-loop regulation of one of the outputs yields excellent regulation of the other output.

The last point in the design guidelines above can be illustrated using the experimental example of Figs. 1 and 2. Couplings among the secondary windings are such that all terms in the first and the third row of $\mathbf{R}'$ have the same sign, as shown in (30) or (34). As a result, the outputs V_2 and V_4 change in the same direction for any change of load currents. In contrast, the signs of the terms corresponding to V_3 and V_4 are opposite. If, for example, the load I_4 increases, the outputs V_4 and V_2 decrease, while the output V_3 increases, as shown in Fig. 8. Suppose now that the output V_4 is closed-loop regulated so that load-induced variations in V_4 are compensated by variations in duty ratio D. From our model we can expect improved cross-regulation on the V_2 output compared to the V_4 output. Fig. 9 shows the measured closed-loop cross-regulation $\Delta V_2(I_4)$, $\Delta V_3(I_4)$, for the converter with passive voltage-clamp snubber. As expected, the total voltage variations on the V_2 output is smaller than on the V_3 output. The winding arrangements that result in opposite-sign terms in the resistance matrix clearly give poor cross-regulation results. A better match between the output resistance terms for the V_2 and V_4 outputs could be obtained by improving the coupling between the primary and the W_4 output, which would result in improved cross-regulation on the V_2 output.

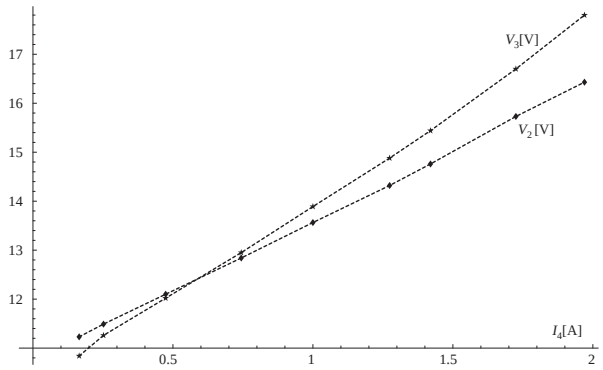

Figure 9: Cross-regulation $V_2(I_4)$ and $V_3(I_4)$ for the case when the auxiliary outputs operate at $I_2 = I_3 = 0.4$A, and the main output load varies between $I_4 = 0.2$A and $I_4 = 2$A. The converter is operated closed-loop at $f_s = 100$kHz, $V_4 = 3.3$V.

6 Conclusions

Operation and characteristics of multiple-output flyback converters depend strongly on the transformer leakage inductances. In particular, steady-state output voltages and cross-regulation properties are determined by how well individual transformer windings are coupled. Taking into account the effects of leakage inductances has been considered intractable in all but the simplest cases limited to two secondary windings or based on other simplifying assumptions about the transformer model. In this paper, complex operation of multiple-output flyback converters is explained in terms of the extended cantilever magnetics model. This general circuit model allows easy qualitative and quantitative explanation of the observed secondary current waveforms, as well as a general steady-state analysis in terms of the extended cantilever model parameters. Two snubber configurations are considered: a passive voltage-clamp snubber and an active-clamp snubber. In both cases, analytical models are derived that can accurately predict steady-state cross-regulation properties of a converter with any number of outputs and with arbitrarily complex magnetics configuration. Predictions of the models are verified by experiments. The analytical models are the basis for a discussion of magnetics design guidelines that can result in improved cross-regulation in multiple-output flyback converters.

References

[1] T. Wilson, Jr,. "Cross regulation in an energy-storage DC-to-DC converter with two regulated outputs," IEEE PESC, 1997 Record, pp. 190-199.

[2] K. Liu, “Effects of leakage inductances on the cross regulation in a discontinuous conduction mode flyback converter,” Proc. High Frequency Power Conversion Conference, 1989, pp. 254-259.

[3] J. Marrero, “Improving cross regulation of multiple output flyback converters,” PCIM 1996.

[4] R. W. Erickson, D. Maksimović, “A multiple-winding magnetics model having directly measurable parameters,” IEEE PESC 1998.

[5] D. Maksimović, R. W. Erickson, C. Griesbach, “Modeling of cross-regulation in converters containing coupled inductors,” IEEE APEC 1998, pp. 350-356.

[6] Uceda & Co. COULD NOT FIND THEM IN PESC’98